Single-molecule force-conductance spectroscopy of hydrogen-bonded complexes

Alessandro Pirrotta,[1] Luca De Vico,[2] Gemma C. Solomon,[1] and Ignacio Franco[3,a)]
[1]*Nano-Science Center and Department of Chemistry, University of Copenhagen, 2100 Copenhagen Ø, Denmark*
[2]*Department of Chemistry, University of Copenhagen, 2100 Copenhagen Ø, Denmark*
[3]*Departments of Chemistry and Physics, University of Rochester, Rochester, New York 14627-0216, USA*

(Received 31 October 2016; accepted 2 February 2017; published online 22 February 2017)

The emerging ability to study physical properties at the single-molecule limit highlights the disparity between what is observable in an ensemble of molecules and the heterogeneous contributions of its constituent parts. A particularly convenient platform for single-molecule studies are molecular junctions where forces and voltages can be applied to individual molecules, giving access to a series of electromechanical observables that can form the basis of highly discriminating multidimensional single-molecule spectroscopies. Here, we computationally examine the ability of force and conductance to inform about molecular recognition events at the single-molecule limit. For this, we consider the force-conductance characteristics of a prototypical class of hydrogen bonded bimolecular complexes sandwiched between gold electrodes. The complexes consist of derivatives of a barbituric acid and a Hamilton receptor that can form up to six simultaneous hydrogen bonds. The simulations combine classical molecular dynamics of the mechanical deformation of the junction with non-equilibrium Green's function computations of the electronic transport. As shown, in these complexes hydrogen bonds mediate transport either by directly participating as a possible transport pathway or by stabilizing molecular conformations with enhanced conductance properties. Further, we observe that force-conductance correlations can be very sensitive to small changes in the chemical structure of the complexes and provide detailed information about the behavior of single molecules that cannot be gleaned from either measurement alone. In fact, there are regions during the elongation that are only mechanically active, others that are only conductance active, and regions where both force and conductance changes as the complex is mechanically manipulated. The implication is that force and conductance provide complementary information about the evolution of molecules in junctions that can be used to interrogate basic structure-transport relations at the single-molecule limit. *Published by AIP Publishing.* [http://dx.doi.org/10.1063/1.4976626]

I. INTRODUCTION

In the quest for unambiguous evidence in support or against a hypothesis, modern spectroscopy often takes advantage of multidimensional strategies to resolve signals that can have multiple causes in linear spectroscopies.[1,2] This is done by considering the response of a system to two or more external stimuli that are applied simultaneously, as their correlation can often resolve ambiguities in the interpretation of the response of a system to a single probe.

At the single-molecule limit,[3–12] a current topical challenge is to implement multidimensional spectroscopies that allow us to examine individual molecules with unprecedented resolution. Such capabilities will considerably enhance our ability to probe, understand, and ultimately control the basic constituents of matter. A particularly convenient platform for multidimensional single-molecule spectroscopies are molecular junctions[9,13–15] where forces, light, and voltages can simultaneously be applied to individual molecules. Here we focus on measurements that investigate the correlation between the electrical and mechanical properties of single molecules in junctions (see, e.g., Refs. 16–29). In this class of measurements, a molecular junction is mechanically deformed while measuring its conductance, or its conductance and the applied force. Experimental techniques that have been developed or adapted for this purpose include low temperature Scanning Tunneling Microscopy (STM),[30–33] STM-break junctions,[18,19,34,35] alpha measurements,[36] and conductive probe atomic force microscopy (CP–AFM).[28,37,38] The utility of this class of multidimensional spectroscopy relies on the fact that conductance and force can offer complementary information about the behavior of single molecules. Conductance probes the electronic structure and transport-determining interactions across the molecule, while force probes the molecular interactions that govern mechanical stability.

In this paper, we computationally investigate the ability of single-molecule force-conductance spectroscopy to probe host-guest molecular recognition events. As an exemplifying case, we focus on the force-conductance properties of the prototypical class of hydrogen-bonded complexes shown in Fig. 1, consisting of a Hamilton-like receptor[39,40] host and a barbituric acid derivative guest. This class of host-guest complexes have been previous employed in developing molecular sensors[39,40] and self-assembly strategies.[41–43] Similar

a)ignacio.franco@rochester.edu

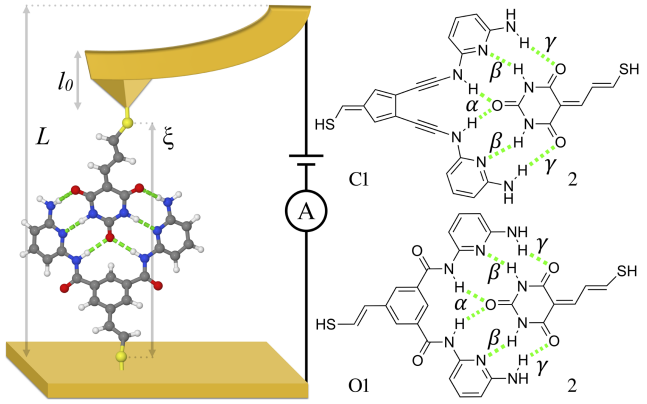

FIG. 1. Scheme of a CP-AFM force-conductance spectroscopy setup (left panel) and of the hydrogen bonded host-guest complexes considered here (right panel). In these experiments, the cantilever-holder-to-surface distance (L) is controlled while the end-to-end molecular distance (ξ) thermally fluctuates. The force $F = -k(\xi + l_0 - L)$ is measured by the deflection of the cantilever from its equilibrium position ($\xi + l_0 - L$), where l_0 is the fixed length of the tip and k is the cantilever stiffness. Simultaneously, the conductance of the molecular junction is measured. The complexes computationally investigated in this setup consist of a Hamilton-like receptor host (C1 and O1) and a barbituric acid derivative guest molecule (2) connected to the gold surfaces of the CP-AFM via thiol-gold bonds. The dashed green lines show the six hydrogen bonds anticipated in the complex, identified with the letters α, β, and γ.

complexes have been synthesized by Glockner.[44] The complexes are thiol-terminated and assumed to be chemisorbed to macroscopic gold surfaces. Through this example, we assess the utility of the force-conductance spectroscopy to provide information about the basic intermolecular interactions that govern supramolecular communication events that are important in a variety of drug design, catalysis, and self-assembly applications. These simulations complement previous studies by us[45] investigating the force spectroscopy of these complexes and their complexation thermodynamics. They also complement conductance experiments that have demonstrated that hydrogen bonds are involved in the electron transfer through molecules[20,46–51] and can sometimes be more conductive than covalent bonds.[52]

Our simulations mimic the CP–AFM force–conductance spectroscopy setup (see Fig. 1). In it, a molecule is attached by its ends to a macroscopic metallic surface and an AFM tip connected to a cantilever. This distance between the surface and the cantilever-holder L is controlled, while the molecular end-to-end distance ξ fluctuates. The fluctuating force $F = -k(\xi + l_0 - L)$ is determined by measuring the deflection of the cantilever ($\xi + l_0 - L$) with respect to its equilibrium position L, where k is the cantilever stiffness and l_0 is the fixed length of the tip. As the molecule is pulled by increasing L, a voltage is applied and both the force on the molecule and the current passing through it are measured. The simulations are performed by combining classical molecular dynamics (MD) of the pulling with electron transport computations using the non-equilibrium Green's function method.

The manuscript is organized as follows: Section II summarizes the MD and electronic transport computational methods employed in the simulations, and the local current analysis used to establish structure-transport relations. Section III discusses the resulting force-conductance spectroscopy, its sensitivity with respect to changes in the chemical structure, and the basic force-conductance behavior that is encountered during junction evolution. In Sec. IV we summarize our main findings and discuss the potential of the approach as a single-molecule multidimensional spectroscopy.

II. THEORETICAL METHODS

A. Molecular dynamics

The classical molecular dynamics strategy and computational setup employed to model the force-spectroscopy have been presented before.[6,45] Briefly, the mechanical deformation of the complexes was simulated in the canonical ensemble (NVT) at 300 K using a Nosé-Hoover chain as a thermostat.[53] The equations of motion were integrated using the modified Beeman's algorithm[54–56] with a 1 fs time step. The force field employed was a modified MM3[57] (with the amide functional group parameters from the MM3-PRO[58]) and a refined set of hydrogen bond parameters previously developed[45] to accurately model hydrogen bonded interactions in the complexes in Fig. 1. The MM3 force field is known to adequately capture π-stacking interactions as required to describe the interactions in the complexes.[59] The MD simulations were carried out with TINKER 6.2.[60] The metal tip and surface were modeled implicitly as impenetrable and rigid parallel surfaces via potential restraints that confine the molecule to the region between the two surfaces. The surfaces were chosen to be perpendicular to the pulling direction and placed at a distance ξ.

The MD computational setup mimics an AFM force-spectroscopy experiment with a cantilever force constant of $k = 110$ pN/Å along the pulling direction and rigid along directions perpendicular to the pulling. The force constant employed is common for AFM cantilevers and softer than the elasticity of gold (800 pN/Å)[36] such that the cantilever deflection, and not the gold's, is dominant during pulling. In the simulations, a zero-length tip ($l_0 = 0$) is considered and the position of the cantilever holder is modeled via a dummy atom. Along the pulling coordinate, the dummy atom is connected via a harmonic spring of stiffness k to one of the molecular terminal S atoms. The position of the other molecular end is fixed throughout the simulation. The deflection of the harmonic spring from its equilibrium position ($\xi - L$) is the simulation equivalent to the cantilever deflection and measures the force $F = -k(\xi - L)$ exerted on the molecule during pulling. The computational setup supposes that the molecule-gold contacts do not migrate during the pulling.

The simulations were performed using a pulling speed of 5×10^{-6} Å/ps. At this speed, the average force-extension isotherms during pulling and subsequent contraction of the complexes essentially coincide, indicating that the system behaves reversibly and the simulation data are independent of the pulling speed.[45] The total simulated MD time was 12 μs.

Cluster analysis in Visual Molecular Dynamics (VMD)[61] was used to determine the most significant conformations during the pulling. This analysis consists in calculating the root mean square deviation (RMSD) of each structure for a given range of ξ with respect to an arbitrary reference (data were

binned in 1 Å intervals). The structures were clustered with respect to their RMSD, determining the likelihood of each.

B. Electron transport

Electron transport across the junction is supposed to be in steady state at each instant of time during the mechanical deformation and well characterized by Landauer coherent transport. Thus, for each MD snapshot, the electronic structure of the system was computed at the Density Functional Tight-Binding (DFTB)[62] level and the energy dependent transmission of the complex was computed using non-equilibrium Green's function method (NEGF).[63] Specifically, the electron transport computations were carried out using the DFTB+NEGF[62,63] software using the *auorg* Slater-Koster parameters[64] developed for describing interactions between organic molecules and gold. We note that due to the finite spatial extent of the basis functions in DFTB, this method is likely to underestimate the long range transmission for the non-covalently bonded complexes considered here.

The transmission at the Fermi energy (which is directly proportional to the zero-bias conductance of the molecule) was computed for 500 randomly selected frames in each 0.1 Å bin from L = 12 Å – 23 Å. For this, explicit gold electrodes were added to the MD snapshots and connected to the terminal thiols. Specifically, the guest and host molecules were chemisorbed on $4\times4\times6$ atom cluster electrodes by removing the thiol hydrogen atoms and placing the sulfur atoms on an fcc(111) hollow site at 2.41 Å distance from the electrode surface. These gold-sulfur distances were held constant for all calculations and chosen according to the literature.[65] Fermi energy of gold was set to −4.6840 eV. The electronic temperature of the electrodes was set to 50 K for smearing the Fermi functions and to ease convergence. The effect on the conductance of changing the contact temperature from 0 K to 300 K was found to be negligible (2%-8% change in $\log(G/G_0)$ for a test set of configurations) with respect to the thermal distribution of conductance values.

C. Local currents

To establish structure-transport relations, a local current analysis was performed as described in Ref. 66. In it, the current is decomposed into inter-atomic contributions, which offers a measure of how much current passes through a particular bond or atom-pair. In the computations, a symmetric 0.1 eV bias was applied in order to decompose the Landauer-Büttiker currents into contributions from atomic pairs. Average local currents are obtained over 0.5 Å bins for each L during the elongation. For definitiveness, we only choose conformations that have a logarithm of the transmission within 25% of the average $\langle\log(G/G_0)\rangle_L$.

III. RESULTS AND DISCUSSION

A. Summary of previous findings

In Ref. 45 we computationally investigated the force-extension ($F-L$) isotherms of the host-guest complexes in Fig. 1 and two other complexes. The $F-L$ curves of these complexes exhibit peaks that signal conformational changes during elongation, the most prominent of which is in the 60–200 pN range and corresponds to the force required to break the hydrogen bonds. These peaks in the $F-L$ curves were found to be sensitive to relatively small changes in the chemical structure of the host molecule. In addition, to obtain thermodynamic insights into the supramolecular assembly, in Ref. 45 we reconstructed from the force data the Helmholtz free energy profile along the extension coordinate and decomposed it into energetic and entropic contributions. The complexation was found to be energetically driven and entropically penalized, with the energy contributions overcoming the entropy penalty and driving molecular recognition. Further, the molecular nanoconfinement introduced by the macroscopic surfaces in this class of experiments was shown to significantly accentuate the mechanical and energetic stability of the hydrogen-bonded complexes, thus enhancing the ability of the force spectroscopy to probe this type of molecular recognition events.

Results presented below augment this picture by offering insights into the conductance behavior and the force-conductance correlations.

B. Force-conductance distributions during elongation

Histograms associated with the force-conductance spectroscopy for complexes C and O are shown in Fig. 2. The figure shows how conductance and force are correlated during the pulling. While the force is plotted individually to the conductance, they are both plotted as a function of a common variable (the end-to-end molecular extension ξ or the surface-to-cantilever holder distance L). As such, these plots convey additional information that is not readily evident in 2D force-conductance histograms of the data (shown in Figs. S1, S2, and S3 in the supplementary material). The generated statistics for both force and conductance have been checked for convergence. Sample probability distributions of $\log(G/G_0)$ during the pulling are included in Fig. S4 of the supplementary material.

Both force and conductance exhibit large scale fluctuations that are comparable to the average values, as is characteristic for single molecules and other systems that are not in the thermodynamic limit (where fluctuations of observables are negligible with respect to average values).[67,68]

The fluctuations in the force reflect conformational changes along the ξ coordinate, while the fluctuations in the transport reveal transport-determining conformational changes within the thermal ensemble. The average behavior of force and conductance is indicated by the lines in Fig. 2. In the case of conductance, two averages are shown as follows: the logarithm of the average $\log\langle G/G_0\rangle$ (dashed lines) and the average of the logarithm $\langle\log(G/G_0)\rangle$ (solid lines). While $\langle\log(G/G_0)\rangle$ follows closely the most probable conductance value, the average conductance is dominated by a few conformations with high conductance properties. The conductance of the minimum energy structure of both complexes is shown by a star in the figure. Note that the conductance properties of the geometrically relaxed structure do not necessarily coincide with the statistical averages, pointing out the importance of taking into account geometrical fluctuations when establishing structure-function relations.

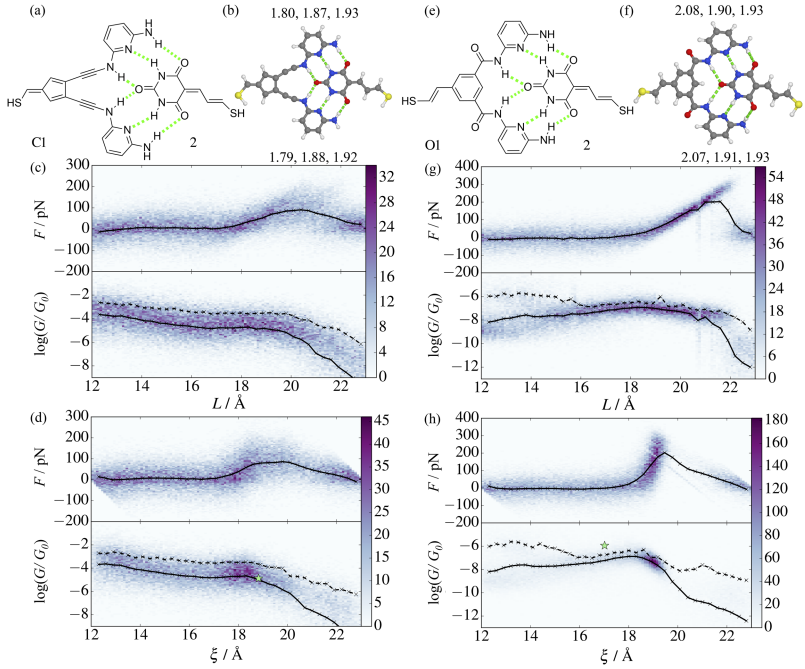

FIG. 2. ((a) and (e)) Chemical structures and ((b) and (f)) optimized molecular structures of complexes C and O in vacuum. The hydrogen bond lengths in the α,β,γ order are reported in Å. ((c), (d), (g), and (h)) 2D histograms of force and conductance versus the cantilever-surface distance L and versus the S-S atoms distance ξ for complexes C and O. The color bar indicates the number of counts in bins of dimension 0.1 Å × 5 pN and 0.1 Å × 0.1 $\log(G/G_0)$. At L and ξ larger than 20.0 Å, a significant probability distribution of frames with zero conductance ($\log(G/G_0) \leq -12$) arises. The star shows the conductance of the minimum energy structure of both complexes, and the lines represent the average behavior. In the case of conductance, two averages are shown as follows: the logarithm of the average $\log\langle G/G_0\rangle$ (dashed lines) and the average of the logarithm $\langle\log(G/G_0)\rangle$ (solid lines).

The results below complement this picture by offering insights into the conductance behavior and the force-conductance correlations.

C. Force-conductance averages

Complexes O and C (*cf.* Fig. 1) can form the same number and type of hydrogen bonds but differ by the central ring of the host molecule 1 and its connection to its two pyridine-based arms. These slight chemical modifications change the mechanical stability and conductance properties of the complex and lead to dramatically different force-conductance properties. These differences are discussed below in terms of the average behavior of the log(conductance) and force measurements (Figures 3(a)–3(d)) together with molecular conformations (top panel of Figure 3) obtained from a cluster analysis of the MD trajectory. We focus on $\langle\log(G/G_0)\rangle$, as opposed to $\log\langle G/G_0\rangle$, because it provides a good estimate of the most probable conductance in the statistical ensemble.

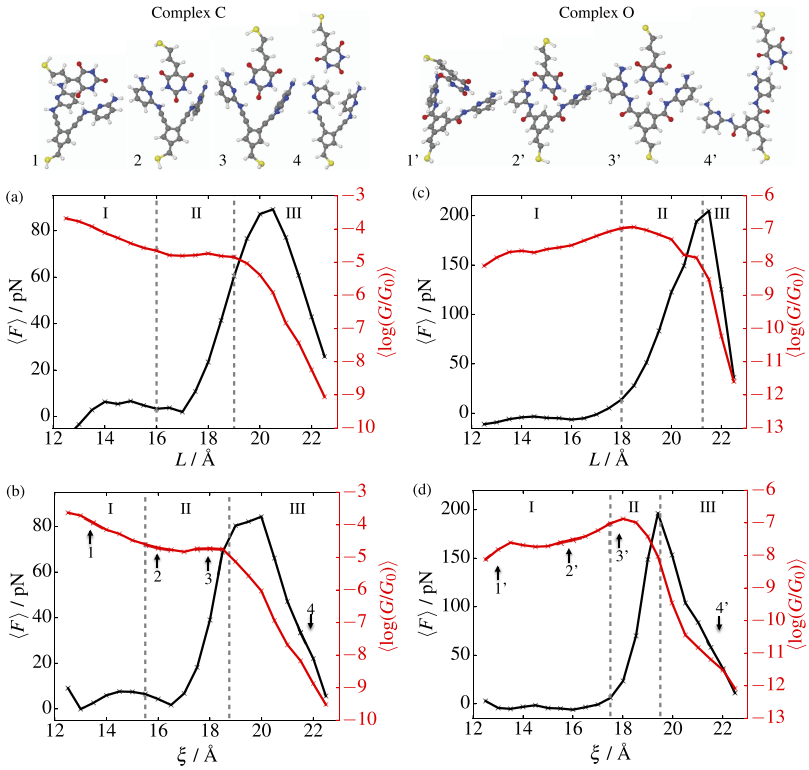

FIG. 3. Average force and log(conductance) versus L and ξ for complex C ((a) and (b)) and complex O ((c) and (d)) in the vicinity of the breaking point. The averages were calculated over a bin of width 0.5 Å. (Top panel) Representative conformations at different molecular lengths ξ during the MD. These structures were selected through a cluster analysis of the trajectory and they represent the most probable structure within 1 Å of ξ.

1. Complex C

During elongation, complex C undergoes a conformational transition from a stacked compact structure ($L \approx 12-16.5$ Å, $\xi \approx 12-16.5$ Å, structure 1) to a hydrogen bonded structure ($L \approx 16.5-19$ Å, $\xi \approx 16.5-18.5$ Å, structures 2, 3) and finally to a mechanically deformed and partially uncomplexed state ($L > 19$ Å, $\xi > 18.5$ Å, structure 4). Representative conformations are shown in the top panel of Figure 3. These three main conformational stages lead to three distinct regions in the force-conductance behavior of this molecule, labeled I, II, and III in Figure 3. Specifically, in region I, the most probable conductance decays exponentially while the force is approximately constant. In region II, the conductance remains approximately constant while the force increases as the hydrogen-bonded conformation is mechanically deformed. In region III, the force reaches its global maximum value and eventually drops. The peak in the force corresponds to the force required to break the hydrogen bonds in the molecule.[45] At this stage of the extension, all hydrogen bonds and any other intermolecular interactions holding the complex together collectively break. This mechanical deformation and eventual rupture of the complex leads to a sharp conductance decay.

Note that the deformation and breaking of the gold contacts observed in related experiments[69] that can give rise to additional peaks in the force typically occur at larger forces (~1 nN) than the molecular events studied here.

2. Complex O

During pulling, complex O undergoes a conformational transition from a V shaped stacked molecule (1′) to a hydrogen bonded structure (2′, 3′) and, subsequently, to an uncomplexed or partially complexed state (4′). For this complex, we can also identify three main regions in its force-conductance behavior. In region I ($L \approx 12-18$ Å, $\xi \approx 12-17.6$ Å), the force remains approximately constant and fluctuates around zero, while the most probable conductance observes exponential growth and reaches its maximum. The maximum in the conductance is achieved when the molecule is planar and thus can form the largest number of intermolecular hydrogen bonds. In region II ($L \approx 18-21.7$ Å, $\xi \approx 17.6-20$ Å), the force increases as the fully formed hydrogen bonded complex is mechanically deformed. The mechanical weakening of the complex leads to a decay in the conductance. Last, in region III ($L > 21.7$ Å, $\xi > 20$ Å) the complex is mechanically broken leading to an abrupt decrease in both force and conductance.

3. Contrasting the two cases

In spite of their chemical similarities, the force-conductance spectroscopy of complexes O and C are quite different. First, the force required to break the hydrogen bonds in complex O (205 pN) is approximately a factor of two larger than the breaking force for complex C (89 pN). This is because, in its planar hydrogen bonded conformation, complex O forms, on average, 2-2.5 times more hydrogen bonds than complex C.[45] Further, the magnitude of the conductance of complex O is much smaller than the one of complex C. As discussed in Sec. III D, this is due to the limited electronic coupling from the electrodes into the arms of O1 because of the *meta*-substitution. Because of this, none of the hydrogen bonds in O can couple to the electrode and that considerably reduces the transmission at the Fermi energy.[70] In addition, the force-conductance correlations in the two complexes are qualitatively different. While in both cases region I is conductance active but mechanically (approximately) inactive, for complex O stretching the stacked conformation leads to an increase of the conductance, while the opposite is observed for complex C. Region II is mechanically active in both cases, but it is only conductance active in complex O. In region III, in both cases the uncomplexation leads to a decay of both force and conductance. This qualitative and quantitative dependence of the force-conductance correlations to the chemical details makes this type of spectroscopy a powerful avenue for single-molecule characterization.

Such differences in the conductance behavior of the two complexes are examined below via an analysis of the local currents.

D. Hydrogen bonds and local currents

While there is no through-bond pathway from one electrode to the other in our complexes, hydrogen bonded systems are known to be able to carry current.[49,51,52,71] However, hydrogen bonds are not the only interactions that hold the complex together, we have also π–π stacking interactions and van der Waals interactions. So, we are left with the following questions: (1) Are the hydrogen bonds the dominant pathway(s) for carrying the current? (2) Is the magnitude of the current correlated with the number of hydrogen bonds formed? As discussed below, in complex C the conductance is mediated by some of the hydrogen bonds, while in complex O there is no correlation between hydrogen bond interactions and the conductance pathway. This difference in transport mechanism and the relative magnitudes of transport of the stacked vs. the hydrogen bonded conformations is the origin of the qualitative differences in the conductance behavior of these chemically similar complexes during elongation.

To address the question of the conduction pathway, we examine the average local currents through these systems and the important hydrogen bonds. In Figs. 4–6, local currents (LCs) are depicted with red arrows on one representative structure from the ensemble of conformations. The width of each arrow is directly proportional to the relative contributions to the current and normalized with respect to the largest element observed. Only LC elements greater than 2% of the total current are shown. To clarify the contributions of hydrogen bonds to the molecular conductance, we define a quantity analogous to the local currents that we call "hydrogen bond fractions" (HBFs). The HBFs are defined as the quotient of the average hydrogen bond binding energy (HBBE) between a given pair of atoms with the largest HBBE possible for that particular HB type (i.e., for O—H 3.5 kcal/mol and N—H 14 kcal/mol).[45] All possible hydrogen bonds have been considered over the same set of molecular conformations that were analyzed for the LCs. These HBFs are plotted with green lines in the same way as was done for the LCs. The width of lines is directly proportional to the HBBE magnitudes. Only HBFs greater than 10% of the maximum HBBE are shown.

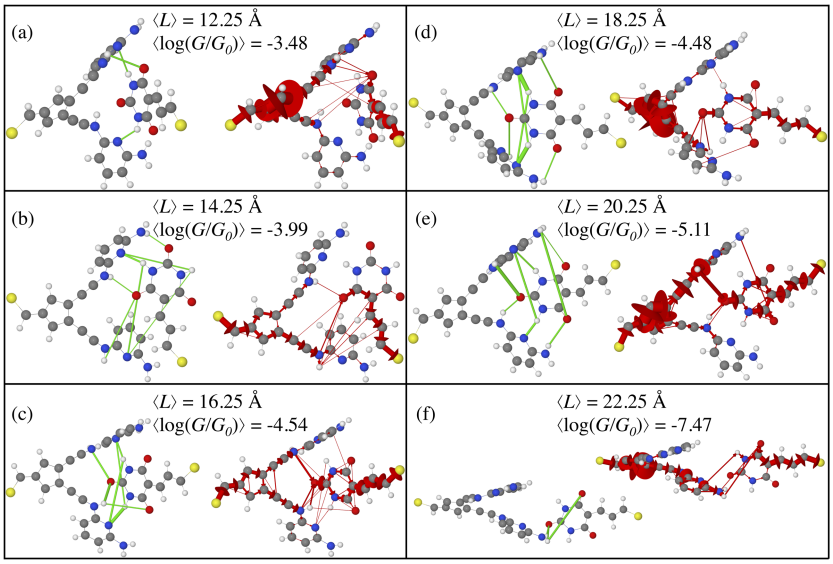

FIG. 4. Complex C: Average hydrogen bond fractions (left, green lines) and local currents (right, red arrows) at different L. To obtain averages, 50 conformers were randomly selected from the MD trajectory over a 0.5 Å bin in L with the only criterion that the log-conductance of the conformer was within 25% of the average $\langle \log(G/G_0) \rangle_L$. Both local currents and relative hydrogen bonds were calculated for each frame and the average was plotted on one of the frames. The width of the arrows (lines) is directly proportional to the relative magnitude of the inter-atomic local currents (hydrogen bond interactions). Note that the large currents observed in some frames in the five-membered ring are predominantly ring currents that are not contributing to the net current.

Figures 4 and 5 show the LCs and HBFs for complexes C and O, respectively, at different points during the extension. When plotting average LCs and HBFs on a fixed conformation, there are interactions between atoms at large (apparently unphysical) distances. The reason for this is because a whole ensemble of conformations was taken into account to obtain averages. To this extent, long range HBFs or LCs should be interpreted as giving a measure of the conformational freedom of the structure. In this discussion, we will employ the α, β, γ convention for the hydrogen bonds specified in Fig. 1. We will refer to the specific hydrogen bond formed by the ith ($i = \alpha, \beta, \gamma$) donor H atom and the jth ($j = \alpha, \beta, \gamma$) acceptor atom as the iD-jA-HB. For example, a hydrogen bond between the amino group (NH_2) of molecule 1 and the central —N—(C═O)—N—carbonyl of molecule 2 will be denoted as γD-αA-HB.

1. Complex C

As can been gleaned from Figure 4, generally, for complex C the LCs and the HBFs involve the same atoms. While there are atomic pairs that are not hydrogen bonded that are involved in the current, and hydrogen bonded pairs that do not carry current, the overall transport pathways approximately match with the important hydrogen bonded contributions in this molecule for all extensions L considered. This suggests that, for this complex, in regions II and III transport is determined by transport through hydrogen bonds.

In additional detail, for complex C at $L = 12.25$ Å only the β-HB and a αD-γA-HB are formed. The LCs show that only the αD-γA-HB carries current. Upon stretching, additional hydrogen bonds form (L = 14.25 Å). Specifically, the guest molecule shuttles between the two pyridine based arms (note the two β-HBs form with both NH groups of the guest). The electron transport is still dominated by the αD-γA-HB. At L = 16.25 Å, a conformation close to the fully hydrogen bonded host-guest complex forms and the current is now injected into the central carbonyl of the guest (through the α-HBs). The drop in conductance can be explained by the different conduction paths in the guest molecule (*cf.* Figure 4(a) with Figure 4(c)). At L = 18.25 Å, two more hydrogen bonds are formed, however the conductance remains unchanged and the LCs indicate no change in the pathway. In the stretched host-guest

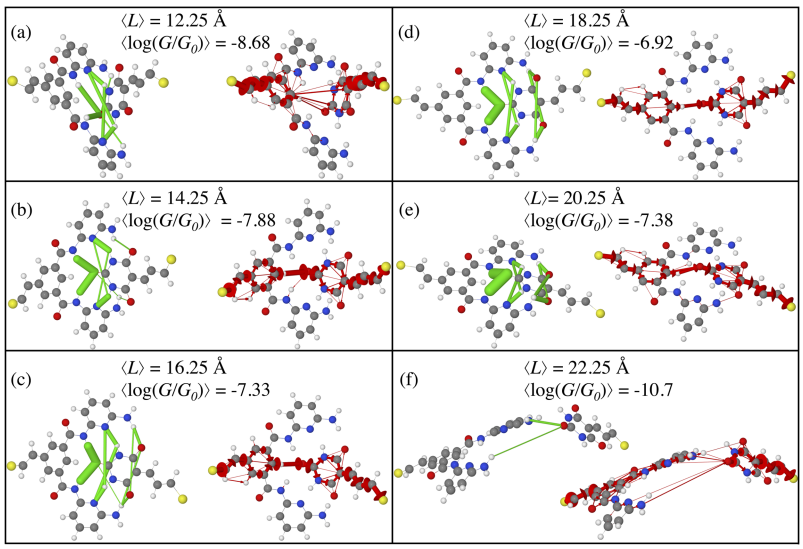

FIG. 5. Complex O: Average hydrogen bond fraction (left, green lines) and local currents (right, red arrows) at different L. The averaging procedure is described in Fig. 4.

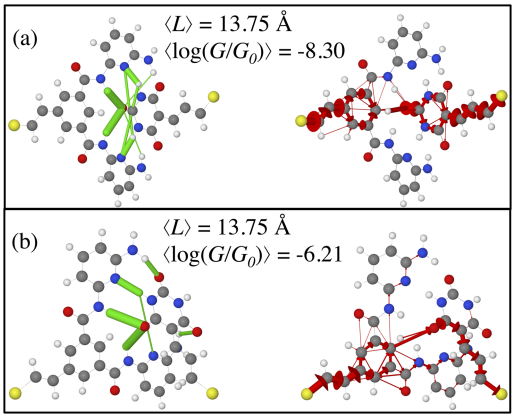

FIG. 6. Representative structures, average relative hydrogen bonds (left, green lines), and local currents (right, red arrows) for complex O in its bistable form around L = 13.75 Å.

complex conformation at L = 20.25 Å, we find an asymmetry in the hydrogen bonds, specifically the upper pyridine based arm (Figure 4(e)) forms stronger or more frequent hydrogen bonds (larger average of HBBEs) than the lower arm. Remarkably the same is also found for the LCs demonstrating that the larger the HBFs, the larger the LCs (albeit not the total current) for this complex. Finally, at longer L the complex breaks and few binding interactions occur (αA-γD-HB and γ-HB).

While the local currents only show us where the current actually flows, rather than giving us the reason why other paths are not favored, we can use this information to ask questions about the potential limitations of alternant paths. In the case of the three sets of hydrogen bonds, we can hypothesize that the dominant role of the α-HBs in carrying the current is due to the absence of meta-substituted rings in the tunneling path for these HBs, a condition that is not fulfilled for the β-HB or γ-HB pathways.

As a separate test of the observation that hydrogen bonds directly participate as a possible transport pathway in complex C, Figure 7 shows a 2D histogram of the hydrogen bond mediated intermolecular interactions and the conductance, using conformations taken just before the peak in the force-conductance isotherm (around ξ = 18 Å). As discussed in Ref. 45, this set of conformations is stabilized by hydrogen bonds. The lines in the plot correspond to the $\langle \log(G/G_0) \rangle$ for different interaction strengths. As shown, the conductance is

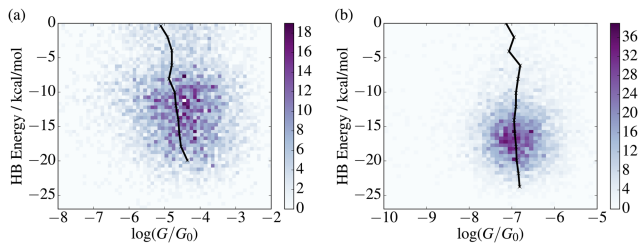

FIG. 7. 2D Histograms of the intermolecular hydrogen bonding interactions (HB energy) versus conductance for (a) complex C and (b) complex O for hydrogen bond stabilized structures (around $\xi = 18 \pm 0.5$ Å). The color bar indicates the number of counts in bins of dimension 0.5 kcal/mol × 0.1 $\log(G/G_0)$. The solid lines indicate the average $\log(G/G_0)$ for varying degrees of HB energy. Note how in complex C the conductance is partially correlated to the degree of hydrogen bonding, while in complex O it is independent of it.

partially correlated with the hydrogen bonding interactions. In fact, the distribution in the 2D histogram is diagonally skewed (this fact is evident both in the distribution and in the averages) indicating that the stronger the hydrogen bonding interactions the higher the conductance. Note that the correlation is not perfect as not all of the hydrogen bonds that can be formed participate in the current.

2. Complex O

As evidenced by Figure 5, and in contrast to complex C, during the extension of complex O the transport is not determined by hydrogen bonds but by the overlap of the π system of the benzene ring (host) with the π system of the guest. Specifically, the transport between the two molecules is determined by the electronic coupling between the benzene ring of the host and the central carbonyl of the guest molecule, which are not hydrogen bonded. In this case, the conductance increases with elongation as the V-shaped complex planarizes because a planar structure leads to a stronger overlap between the two π-systems. After L = 18.25 Å, the molecules are pulled apart and the conductance decreases upon further stretching.

In additional detail, at L = 12.25 Å four hydrogen bonds participate of the dynamics: two α and two β-HBs. As the complex is stretched, no hydrogen bonds are broken; the guest and host molecule pivot in opposite directions around the two β-HBs allowing the formation of the two γ-HBs. Throughout the whole pulling process, the conductance is mediated by the π-systems of the donor and acceptor. The conductance increases upon stretching (from Figs. 5(a)–5(d)), reaching its maximum value at L = 18.25 Å. At this L the fully hydrogen bonded structure is reached. Thus, in this case, while hydrogen bonds do not actively participate in the current they do stabilize a conformation where the orbital overlap between the donor and acceptor enhances transport. This conclusion is also evident in Fig. 7, that shows that for complex O the conductance is uncorrelated with the strength of the hydrogen bonding interactions for conformations around ξ = 18 Å that are stabilized by hydrogen bonds.

Figures 2(g) and 2(h) show a bistability in the conductance for complex O at L (ξ) ≈ 14 Å. This bistability arises because there are two distinct ensembles of conformations that have a conductance difference of two orders of magnitude. Figure 6 shows representative structures and the LCs and HBFs for these two sets. As shown, this difference arises because in the conformers of higher conductance the tunneling path is significantly shorter due to the relative position of the guest and host molecules.

IV. FINAL REMARKS

In this paper, we have numerically investigated the force-conductance signatures of molecular recognition events through hydrogen bonding, using the supramolecular complex shown in Fig. 1 as an exemplifying case. The simulations indicate that force-conductance correlations can provide detailed information about the behavior of single molecules that cannot be gleaned from either measurement alone. This is because force and conductance are complementary techniques; conductance probes the electronic structure of the molecule in

a junction, while force-measurements probe the intramolecular and intermolecular interactions which are responsible for mechanical stability. Further, while force-spectroscopy allows for mechanical control over molecular conformation with sub-Angstrom resolution, conductance measurements permit monitoring with exponential sensitivity transport-determining changes in conformation. Such exponential sensitivity arises from the fact that electron transport through small molecules occurs through quantum mechanical tunneling.

The supposition in the simulations is that the transport is well described by the Landauer formula. In any conformationally flexible system, incoherent transport may also be present and can contribute to the overall current. Thus, the reported conductances should be interpreted in a qualitative sense. They serve as a proxy to investigate the general question of whether the interactions that favor binding necessarily also favor transport. Landauer transport gives a simple picture of the electronic coupling between the leads across the molecule and it is the evolution of this coupling that we probe.

Our view is that force-conductance measurements have the potential to become a useful multidimensional single-molecule spectroscopy. In fact, in the case of the complexes considered, there were clear regions in the elongation that are only mechanically active, others that are only conductance active, and regions where both force and conductance change as the complex is mechanically manipulated. In addition, we find that elongating the supramolecular complex without breaking it can either increase (complex O) or decrease (complex C) the most probable conductance value. Further, bistable conductance regimes can be seen in regions where the force does not exhibit bistability. The implication of this series of observations is that force and conductance are sensitive to different types of changes in molecular conformation and, together, provide a richer understanding of the behavior of single molecules in junctions.

Further, we have observed that force-conductance spectroscopy can be very sensitive to details in the chemical structure. In fact, while the two complexes studied here are seemingly very similar, small changes in the structure can have both qualitative and quantitative impact on the force, the conductance, and the force-conductance correlation. At the qualitative level, at least three different regions have been identified in the two complexes considered here from the trend of force and conductance upon elongation (Fig. 3). We can expand these findings by taking into account all possible combinations of how a change in molecular conformation can give a specific trend in the force or conductance signal under elongation. Figure 8 shows all these combinations: $\partial F/\partial L$ and $\partial \log G/\partial L$ equal, greater, or smaller than zero. An equivalent diagram can be made using the molecular elongation ξ as a variable. For instance, case 4 vs. case 6 was observed in region I for complex C vs. complex O; case 1 vs. case 2 in region II. Other combinations could be measured in different molecules, and each one tells a different molecular story of the junction evolution.

While Fig. 8 highlights the changing contributions of the two signals in a particular region, it is clear that the observed sequence of regions also provides additional information. In a theoretical study such as this, it is generally possible to backtrack from the calculated observable to the atomistic details and rationalize the structure-function relationships that are observed. In an experiment, however, the details of the structural evolution of a flexible system under strain will generally be unknown. It remains to be seen whether the combination of changing force and conductance data will be sufficient to identify the structural motifs observed during a pulling experiment, but there seems to be scope to expect a characteristic fingerprint from families of molecules as the system moves between regions in Fig. 8.

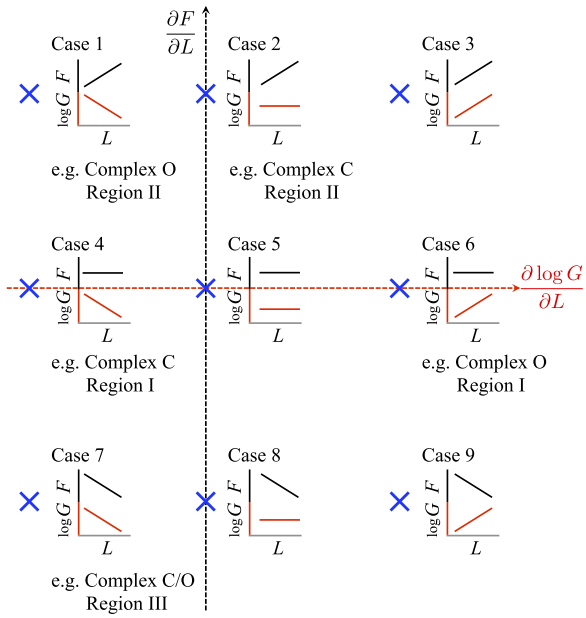

FIG. 8. Different scenarios of the force and conductance trend versus the pulling coordinate. The dashed axes correspond to the derivative of force and conductance, respectively. Nine possible cases are shown and where possible the case is linked to the results shown in Fig. 3.

In the context of supramolecular complexes, an advantage of this type of spectroscopy is that the nanoconfinement of the molecular system between the AFM tip and the surface enhances the mechanical stability and the complexation energy of the dimer.[45] That is, nanoconfinement enhances the sensitivity of the force-conductance spectroscopy to molecular recognition events. In the complexes considered, hydrogen bonds were seen to mediate transport either by directly participating as a possible transport pathway as revealed by local currents and energetic considerations (complex C), or by stabilizing molecular conformations with enhanced conductance properties (complex O).

Naturally, there are challenges that need to be overcome to further advance this route for multidimensional single-molecule spectroscopy. A basic experimental challenge is the lack of control of the junction configuration in break-junction experiments. This uncertainty in the conformation typically leads to an analysis based on statistical averages that do not necessarily reflect the behavior of single molecules. From a simulation perspective, a significant challenge is how to overcome the 6-10 orders of magnitude gap between the pulling speeds that are employed in experiments (nm/s) with those that can be achieved *in silico*. In spite of these challenges, this type of measurements provides a powerful avenue for the manipulation and interrogation of basic chemical and

physical events, such as chemical reactions, molecular recognitions, and conformational dynamics.

SUPPLEMENTARY MATERIAL

See supplementary material for 2D force-conductance histograms of the data.

ACKNOWLEDGMENTS

This work was supported by the University of Rochester startup funds. A.P., L.D.V., and G.C.S. acknowledge financial support from the Danish Council for Independent Research, Natural Sciences and the Carlsberg Foundation. A.P. thanks Gabriele Penazzi for helpful conversations and comments.

[1] S. Mukamel, *Principles of Nonlinear Optical Spectroscopy* (Oxford University Press, 1999).
[2] R. R. Ernst, G. Bodenhausen, A. Wokaun *et al.*, *Principles of Nuclear Magnetic Resonance in One and Two Dimensions* (Clarendon Press, Oxford, 1987), Vol. 14.
[3] W. E. Moerner, Rev. Mod. Phys. **87**, 1183 (2015).
[4] K. C. Neuman and A. Nagy, Nat. Methods **5**, 491 (2008).
[5] M. Rief, M. Gautel, F. Oesterhelt, J. M. Fernandez, and H. E. Gaub, Science **276**, 1109 (1997).
[6] I. Franco, M. A. Ratner, and G. C. Schatz, "Single-molecule pulling: Phenomenology and interpretation," in *Nano and Cell Mechanics*, edited by H. Espinosa and G. Bao (Wiley, 2014), Chap. 14, pp. 359–388.
[7] S. Block, A. Greinacher, C. A. Helm, and M. Delcea, Soft Matter **10**, 2775 (2014).
[8] J. K. Gimzewski, Science **283**, 1683 (1999).
[9] J. P. Bergfield and M. A. Ratner, Phys. Status Solidi **250**, 2249 (2013).
[10] A. C. Aragonès, N. L. Haworth, N. Darwish, S. Ciampi, N. J. Bloomfield, G. G. Wallace, I. Diez-Perez, and M. L. Coote, Nature **531**, 88 (2016).
[11] B. Schuler, S. Fatayer, F. Mohn, N. Moll, N. Pavliček, G. Meyer, D. Peña, and L. Gross, Nat. Chem. **8**, 220 (2016).
[12] E. C. Le Ru and P. G. Etchegoin, Annu. Rev. Phys. Chem. **63**, 65 (2012).
[13] E. Scheer, *Molecular Electronics: An Introduction to Theory and Experiment* (World Scientific, 2010), Vol. 1.
[14] F. Chen and N. J. Tao, Acc. Chem. Res. **42**, 573 (2009).
[15] M. S. Hybertsen and L. Venkataraman, Acc. Chem. Res. **49**, 452 (2016).
[16] T. A. Su, H. Li, M. L. Steigerwald, L. Venkataraman, and C. Nuckolls, Nat. Chem. **7**, 215 (2015).
[17] J. J. Parks, A. R. Champagne, T. A. Costi, W. W. Shum, A. N. Pasupathy, E. Neuscamman, S. Flores-Torres, P. S. Cornaglia, A. A. Aligia, C. A. Balseiro, G. K.-L. Chan, H. D. Abruna, and D. C. Ralph, Science **328**, 1370 (2010).
[18] L. Venkataraman, J. E. Klare, I. W. Tam, C. Nuckolls, M. S. Hybertsen, and M. L. Steigerwald, Nano Lett. **6**, 458 (2006).
[19] C. Li, I. Pobelov, T. Wandlowski, A. Bagrets, A. Arnold, and F. Evers, J. Am. Chem. Soc. **130**, 318 (2008).
[20] S. Chang, J. He, A. Kibel, M. Lee, O. Sankey, P. Zhang, and S. Lindsay, Nat. Nanotechnol. **4**, 297 (2009).
[21] W. Hong, H. Valkenier, G. Mészáros, D. Z. Manrique, A. Mishchenko, A. Putz, P. M. García, C. J. Lambert, J. C. Hummelen, and T. Wandlowski, Beilstein J. Nanotechnol. **2**, 699 (2011).
[22] I. Franco, G. C. Solomon, G. C. Schatz, and M. A. Ratner, J. Am. Chem. Soc. **133**, 15714 (2011).
[23] I. Franco, C. B. George, G. C. Solomon, G. C. Schatz, and M. A. Ratner, J. Am. Chem. Soc. **133**, 2242 (2011).
[24] S. M. Parker, M. Smeu, I. Franco, M. A. Ratner, and T. Seideman, Nano Lett. **14**, 4587 (2014).
[25] W. Hong, D. Z. Manrique, P. Moreno-García, M. Gulcur, A. Mishchenko, C. J. Lambert, M. R. Bryce, and T. Wandlowski, J. Am. Chem. Soc. **134**, 2292 (2012).
[26] X. Li, J. He, J. Hihath, B. Xu, S. M. Lindsay, and N. Tao, J. Am. Chem. Soc. **128**, 2135 (2006).
[27] A. Mishchenko, L. A. Zotti, D. Vonlanthen, M. Bürkle, F. Pauly, J. C. Cuevas, M. Mayor, and T. Wandlowski, J. Am. Chem. Soc. **133**, 184 (2011).
[28] B. Q. Xu, X. L. Li, X. Y. Xiao, H. Sakaguchi, and N. J. Tao, Nano Lett. **5**, 1491 (2005).
[29] X. Zhao, C. Huang, M. Gulcur, A. S. Batsanov, M. Baghernejad, W. Hong, M. R. Bryce, and T. Wandlowski, Chem. Mater. **25**, 4340 (2013).
[30] C. Nacci, F. Ample, D. Bleger, S. Hecht, C. Joachim, and L. Grill, Nat. Commun. **6**, 7397 (2015).
[31] M. Koch, F. Ample, C. Joachim, and L. Grill, Nat. Nanotechnol. **7**, 713 (2012).
[32] L. Lafferentz, F. Ample, H. Yu, S. Hecht, C. Joachim, and L. Grill, Science **323**, 1193 (2009).
[33] N. Fournier, C. Wagner, C. Weiss, R. Temirov, and F. S. Tautz, Phys. Rev. B **84**, 035435 (2011).
[34] B. Xu, Science **301**, 1221 (2003).
[35] S. Y. Quek, M. Kamenetska, M. L. Steigerwald, H. J. Choi, S. G. Louie, M. S. Hybertsen, J. B. Neaton, and L. Venkataraman, Nat. Nanotechnol. **4**, 230 (2009).
[36] H. Rascón-Ramos, J. M. Artés, Y. Li, and J. Hihath, Nat. Mater. **14**, 517 (2015).
[37] M. Frei, S. V. Aradhya, M. Koentopp, M. S. Hybertsen, and L. Venkataraman, Nano Lett. **11**, 1518 (2011).
[38] D. J. Wold and C. D. Frisbie, J. Am. Chem. Soc. **123**, 5549 (2001).
[39] S. K. Chang and A. D. Hamilton, J. Am. Chem. Soc. **110**, 1318 (1988).
[40] S. K. Chang, D. Van Engen, E. Fan, and A. D. Hamilton, J. Am. Chem. Soc. **113**, 7640 (1991).
[41] S. K. Yang and S. C. Zimmerman, Isr. J. Chem. **53**, 511 (2013).
[42] A. Dirksen, U. Hahn, F. Schwanke, M. Nieger, J. N. H. Reek, F. Vögtle, and L. De Cola, Chem. - Eur. J. **10**, 2036 (2004).
[43] F. Wessendorf, J.-F. Gnichwitz, G. H. Sarova, K. Hager, U. Hartnagel, D. M. Guldi, and A. Hirsch, J. Am. Chem. Soc. **129**, 16057 (2007).
[44] C. Glockner and U. Lüning, J. Inclusion Phenom. Macrocyclic Chem. **71**, 239 (2011).
[45] A. Pirrotta, G. C. Solomon, and I. Franco, J. Phys. Chem. C **120**, 19470 (2016).
[46] S. Huang, S. Chang, J. He, P. Zhang, F. Liang, M. Tuchband, S. Li, and S. Lindsay, J. Phys. Chem. C **114**, 20443 (2010).
[47] S. Lindsay, J. He, O. Sankey, P. Hapala, P. Jelinek, P. Zhang, S. Chang, and S. Huang, Nanotechnology **21**, 262001 (2010).
[48] S. Chang, J. He, P. Zhang, B. Gyarfas, and S. Lindsay, J. Am. Chem. Soc. **133**, 14267 (2011).
[49] T. Nishino, N. Hayashi, and P. T. Bui, J. Am. Chem. Soc. **135**, 4592 (2013).
[50] Y. Zhao, B. Ashcroft, P. Zhang, H. Liu, S. Sen, W. Song, J. Im, B. Gyarfas, S. Manna, S. Biswas, C. Borges, and S. Lindsay, Nat. Nanotechnol. **9**, 466 (2014).
[51] S. Chang, S. Huang, H. Liu, P. Zhang, F. Liang, R. Akahori, S. Li, B. Gyarfas, J. Shumway, B. Ashcroft, J. He, and S. Lindsay, Nanotechnology **23**, 235101 (2012).
[52] M. Wimmer, J. L. Palma, P. Tarakeshwar, and V. Mujica, J. Phys. Chem. Lett. **7**, 2977 (2016).
[53] W. G. Hoover, Phys. Rev. A **31**, 1695 (1985).
[54] P. Schofield, Comput. Phys. Commun. **5**, 17 (1973).
[55] D. Beeman, J. Comput. Phys. **20**, 130 (1976).
[56] M. Levitt, H. Meirovitch, and R. Huber, J. Mol. Biol. **168**, 617 (1983).
[57] N. L. Allinger, Y. H. Yuh, and J. H. Lii, J. Am. Chem. Soc. **111**, 8551 (1989).
[58] J. H. Lii and N. L. Allinger, J. Comput. Chem. **12**, 186 (1991).
[59] I. Franco, M. A. Ratner, and G. C. Schatz, J. Phys. Chem. B **115**, 2477 (2011).
[60] J. W. Ponder and F. M. Richards, J. Comput. Chem. **8**, 1016–1024 (1987).
[61] W. Humphrey, A. Dalke, and K. Schulten, J. Mol. Graphics **14**, 33 (1996).
[62] B. Aradi, B. Hourahine, and T. Frauenheim, J. Phys. Chem. A **111**, 5678 (2007).
[63] A. Pecchia, G. Penazzi, L. Salvucci, and A. Di Carlo, New J. Phys. **10**, 65022 (2008).
[64] A. Fihey, C. Hettich, J. Touzeau, F. Maurel, A. Perrier, C. Köhler, B. Aradi, and T. Frauenheim, J. Comput. Chem. **36**, 2075 (2015).
[65] A. Bilić, J. R. Reimers, N. S. Hush, A. Bilic, J. R. Reimers, and N. S. Hush, J. Chem. Phys. **122**, 094708 (2005).
[66] G. C. Solomon, C. Herrmann, T. Hansen, V. Mujica, and M. A. Ratner, Nat. Chem. **2**, 223 (2010).
[67] C. Bustamante, J. Liphardt, and F. Ritort, Phys. Today **58**(7), 43 (2005).
[68] T. L. Hill, *Thermodynamics of Small Systems* (Courier Corporation, 1963).
[69] S. V. Aradhya and L. Venkataraman, Nat. Nanotechnol. **8**, 399 (2013).
[70] P. Sautet and C. Joachim, Chem. Phys. Lett. **153**, 511 (1988).
[71] Y. Li, X. Tu, M. Wang, H. Wang, S. Sanvito, and S. Hou, J. Chem. Phys. **141**, 174702 (2014).